Nano Res. 2011, 4(8): 780–787
DOI 10.1007/s12274-011-0134-9
Research Article

ISSN 1998-0124
CN 11-5974/O4

Synthesis of Monodisperse $CoPt_3$ Nanocrystals and Their Catalytic Behavior for Growth of Boron Nanowires

Yuan Tian[1], Chengmin Shen[1], Chen Li[1], Xuezhao Shi[1,2], Yuan Huang[1], and Hongjun Gao[1] (✉)

[1] Beijing National Laboratory for Condensed Matter Physics, Institute of Physics, Chinese Academy of Sciences, Beijing 100190, China
[2] College of Chemistry and Engineering, Lanzhou University, Lanzhou 730000, China

Received: 23 November 2010 / Revised: 29 March 2011 / Accepted: 29 March 2011

ABSTRACT

Monodisperse $CoPt_3$ nanocrystals (NCs) have been synthesized in oleylamine solution by an organic solvothermal method. The NCs were ellipsoidal particles with a diameter around 6.6 nm and length around 10 nm with a good single crystal structure. Using $CoPt_3$ NCs as catalysts, large-area boron nanowires with diameters ranging from 30 to 50 nm were successfully prepared by chemical vapor deposition using a $C/B/B_2O_3$ mixture as the precursor. Structural analysis indicated that these nanowires were single crystalline with a β-rhombohedral structure. Measurement of the field emission properties of boron nanowire films showed that the boron nanowires have good field emission characteristics.

KEYWORDS

$CoPt_3$ nanoparticles, catalytic behavior, boron nanowires, field emission properties

1. Introduction

Magnetic nanocrystals (NCs) have attracted much attention due to their unique physical and chemical properties and potential applications in ultrahigh density magnetic recording media [1, 2], catalysis [3–5], biological labeling [6, 7], and magnetic resonance imaging [8, 9]. Among these nanocrystals, CoPt bimetallic alloy NCs are an important material by virtue of their high anisotropy, chemical stability, high Curie temperature [10–13], and good electrocatalytic activity [14–16]. Such properties allow these bimetallic magnetic NCs to be not only employed in magnetic recording devices but also as catalysts to grow one-dimensional nanostructured materials. It has been found that their catalytic activity can be improved by modifying their electronic and surface properties [17]. Most recently, the preparation of carbon nanotubes (CNTs) using bimetallic magnetic NCs as catalysts has been reported by several different research groups—for example, Kockrick et al. prepared magnetic MPt nanoparticles inside the pores of ordered mesoporous silica and carbon materials as advanced bifunctional catalysts [18], and Schäffel et al. obtained homogenous and clean CNTs using FePt nanoparticles as catalyst particles [19]. Similarly, vertically aligned carbon nanofibers [20], multiwalled CNTs [21], and single- or double-walled CNTs [22] have also been prepared using different bimetallic magnetic nanoparticles as catalysts. In general, previous research indicates that control over the size, shape, and composition of bimetallic magnetic NCs is very important for controlled aggregation of NCs in the synthesis of one-dimensional nanostructured materials [23], and

Address correspondence to hjgao@iphy.ac.cn

this remains a challenging problem. In the last few years, much effort has been devoted to developing new synthesis techniques for CoPt nanocrystals, including simultaneous reduction of platinum(II) acetylacetonate ($Pt(acac)_2$) and decomposition of $Co_2(CO)_8$ in organic solvents [24, 25], polyol-reduction of $Pt(acac)_2$ and $Co(CH_3COO)_2$ [26, 27], and co-reduction of $CoCl_2$ and $PtCl_2$ using strong reducing agents in phenyl ether solution [28].

Here, we report the successful synthesis of monodisperse $CoPt_3$ NCs in oleylamine at 300 ℃. Unlike previous work, here oleylamine plays a critical role, as reaction solvent, surfactant, and co-reducing reagent in the process of the formation of $CoPt_3$ NCs. This is a simple route to synthesize metal NCs with the usual phenyl ether solvent replaced by oleylamine at a lower cost. The resulting ellipsoidal $CoPt_3$ NCs have a narrow size distribution very near 6.6 nm in diameter and 10 nm in length. Using monodisperse $CoPt_3$ NCs as catalysts, large area boron nanowires (BNWs) have been synthesized through a simple chemical vapor deposition (CVD) method. This is the first report of the utilization of CoPt NCs for the synthesis of BNWs. Due to their lower eutectoid temperature, $CoPt_3$ NCs can achieve better catalytic activity than Fe_3O_4 NPs, while reducing the cost of BNW synthesis compared with that when using pure Pt NPs. The diameters of the BNWs ranged from 30 to 50 nm and were single crystalline with a β-rhombohedral structure. Measurement of their field emission properties showed that BNWs prepared this way are a promising candidate for use in cool cathode devices.

2. Experimental

2.1 Materials

Cobalt(III) acetylacetonate ($Co(acac)_3$), platinum(II) acetylacetonate ($Pt(acac)_2$), oleylamine (OAm), hexane, and 1,2-hexadecandiol were purchased from Sigma–Aldrich. All chemical reagents were used without further purification.

2.2 Synthesis of $CoPt_3$ nanocrystals

1.0 mmol of $Co(acac)_3$, 1.5 mmol of $Pt(acac)_2$, 10 mmol of 1,2-hexadecandiol, 0.5 mmol of oleic acid, and 20 mL of oleylamine were mixed in a 100 mL flask and stirred under a flow of nitrogen at 120 ℃ for 20 min. Then this mixed solution was heated to reflux at 300 ℃ for 2 h. The solution was cooled down to room temperature after removing the heat source. 40 mL of ethanol was added into the solution, and $CoPt_3$ particles were separated by centrifugation at 8000 r/min for 5 min. The as-prepared $CoPt_3$ particles were dispersed in hexane.

2.3 Fabrication of boron nanowires with $CoPt_3$ NCs as a catalyst

B powder (99.9%), B_2O_3 powder (99.99%), and carbon powder (99.9%) with mass ratio of 4:2:1 were milled together. Then this precursor mixture was transferred into an alumina boat. 50 μL of $CoPt_3$ NCs solution in hexane (15 mg/mL) was dropped on the surface of a Si (111) wafer and dried in air. The $CoPt_3$ NCs-covered Si (111) wafer was placed in an alumina boat, lying in front of the precursor mixture. Then the alumina boat was put into a horizontal tube furnace. When the system was pumped below 10 Pa, a H_2/Ar mixed gas (10%, *v*/*v*%) was introduced at a flow rate of 50 sccm (sccm denotes cubic centimeters per minute at STP) for 30 min which was subsequently decreased to 30 sccm. The system pressure was increased to 3×10^2 Pa. Then the furnace was heated to 1100 ℃ at a rate of 5 ℃/min and the system pressure was maintained at 8×10^3 Pa. After reaction for 2 h, the furnace was cooled down to room temperature at a rate of 5 ℃/min. A brown-black product was found on the Si substrate.

2.4 Characterization

Morphologies of samples were examined by field-emission type scanning electron microscopy (FE-SEM) (XL30 SFEG, FEI Corp.). The size and crystal structure of $CoPt_3$ nanocrystals were observed by transmission electron microscopy (TEM) (JEM-200CX, JEOL Corp.) and high-resolution transmission electron microscopy (HRTEM) (Tecnai G2 F20, FEI Corp.). X-ray diffraction (XRD) patterns were recorded on a Rigaku D/max-RC X-ray diffractometer using Cu *K*α radiation ($\lambda = 1.540$ Å). The mapping images of NCs were determined using HRTEM. The magnetic properties of $CoPt_3$ particles were measured by a high sensitivity vibrating sample

magnetometer (VSM) (Model 7404, Lakeshore) with fields up to 1.5 Tesla at room temperature.

3. Results and discussion

The $CoPt_3$ NCs were prepared by simultaneous reduction of $Pt(acac)_2$ and $Co(acac)_3$ using oleylamine as a solvent, which also contained oleic acid and 1,2-hexadecandiol. The morphology and size of $CoPt_3$ NCs were analyzed by TEM and HRTEM. Figure 1 shows a TEM image of $CoPt_3$ NCs. It can be seen that $CoPt_3$ NCs have good monodispersivity. Each nanocrystal is separated from its neighbors by an organic ligand (oleic acid and oleylamine) shell. Unlike the spherical shape of $CoPt_3$ NCs reported in previous work, the shape the $CoPt_3$ NCs is ellipsoidal. The average diameter and length of NCs were 6.6 nm and 10 nm respectively. The HRTEM image of a single $CoPt_3$ (inset of Fig. 1) shows that the nanocrystal has a single crystalline structure without observable defects. The lattice fringes have a separation of approximately 0.231 nm, which is close to interplanar distance of the {111} planes in the face-centered cubic structured $CoPt_3$.

The X-ray diffraction pattern of $CoPt_3$ NCs is shown in Fig. 2. $CoPt_3$ NCs show the typical fcc structure with diffraction peaks at 40.27°, 46.88°, 68.11°, 82.56°, and 87.10°, corresponding to (111), (200), (220), (311), and (222) crystal planes of bulk $CoPt_3$, respectively. The

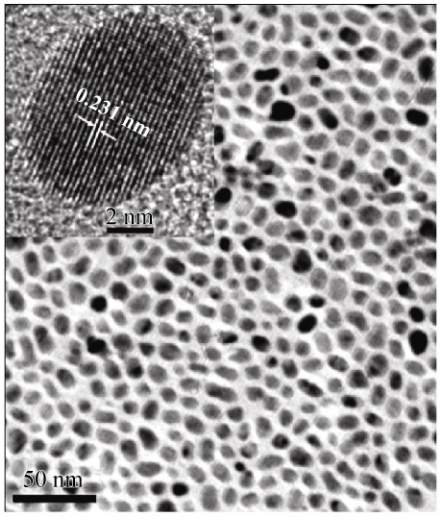

Figure 1 TEM image of $CoPt_3$ NCs prepared using oleylamine as solvent. Which shows that the $CoPt_3$ NCs have narrow size distribution. The inset of the figure shows a HRTEM image

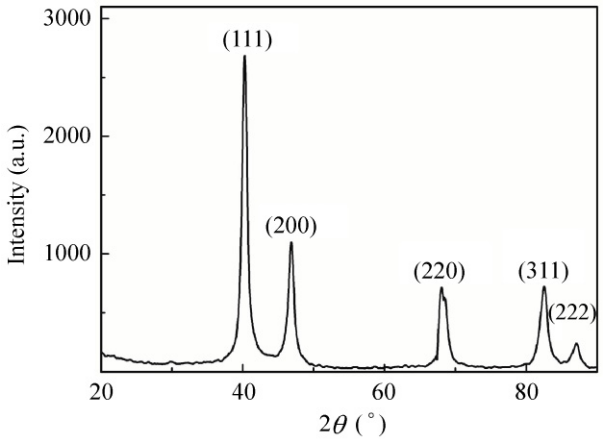

Figure 2 XRD pattern of monodisperse $CoPt_3$ NCs. The $CoPt_3$ NCs have *fcc* crystal structure

strong and sharp diffraction peaks indicate $CoPt_3$ NCs have a good crystallinity.

In order to confirm the composition of the $CoPt_3$ NCs, energy-dispersive X-ray spectroscopy (EDX) was used to analyze the atomic ratio between the Co and Pt in the NCs. The result is shown in Fig. 3(a). The atomic ratio of Co to Pt is 27:73, nearly 1:3. Further measurement was carried out by scanning transmission electron microscopy combined with energy dispersive X-ray spectroscopy (STEM-EDX) line scans to study the distribution of Co and Pt in the $CoPt_3$ NCs (Fig. 3(b)). It can be seen clearly that the $CoPt_3$ NCs show single Gaussian distributions of X-rays across the particle for both elements. Figures 3(c) and 3(d) are STEM-EDX line scan patterns of Pt and Co, respectively. Both elements are uniformly distributed in the NCs, which reveals that the NCs are alloys.

The magnetic properties of $CoPt_3$ NCs were investigated using VSM. A plot of the magnetization of $CoPt_3$ NCs as a function of the applied field at room temperature (300 K) is shown in Fig. 4. The $CoPt_3$ NCs showed superparamagnetic characteristics. The magnetization of $CoPt_3$ NCs reached 20 emu/g, which is consistent with previous reports.

One important application of magnetic NCs is as a catalyst to grow one-dimensional nanostructured materials in a CVD system. Nevertheless, there have been few reports of the $CoPt_3$ NC-catalyzed preparation of one-dimensional nanostructured materials. In the present work, we successfully prepared single crystalline BNW films with a pure β-rhombohedral

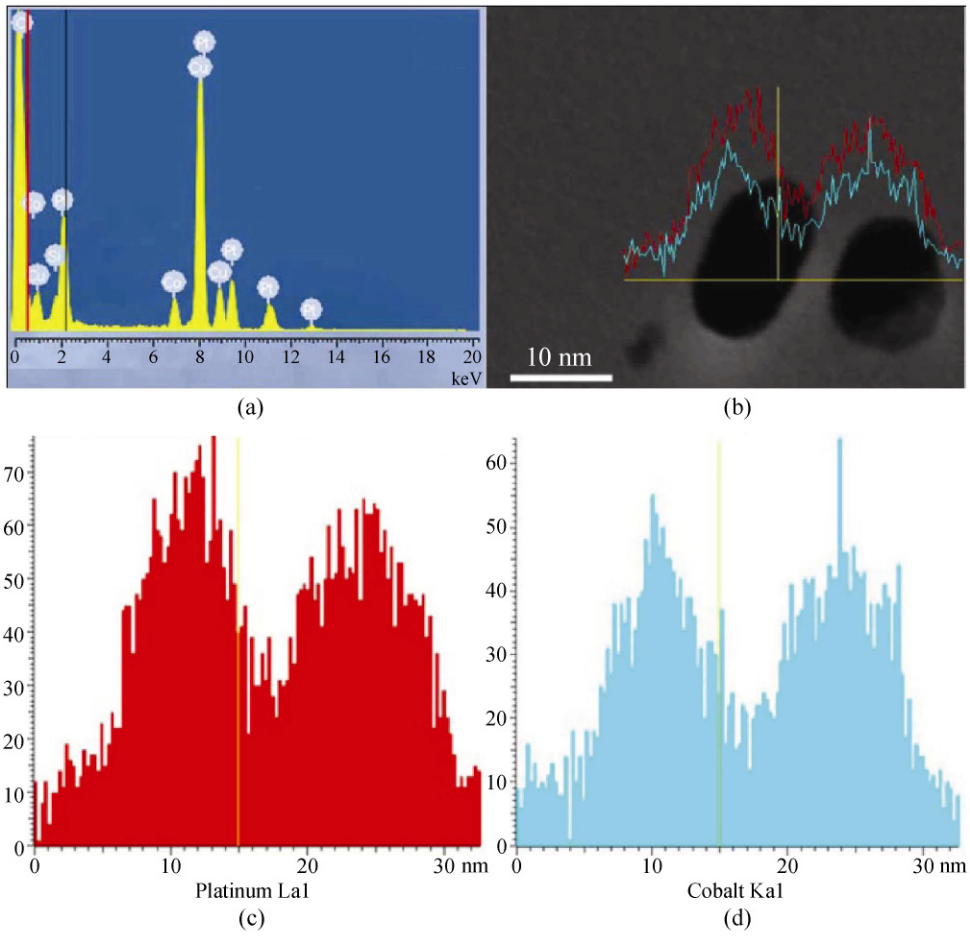

Figure 3 Energy-dispersive X-ray spectra and STEM-EDX line spectra of $CoPt_3$ NCs, indicating that the atomic ratio of Co to Pt is 1:3

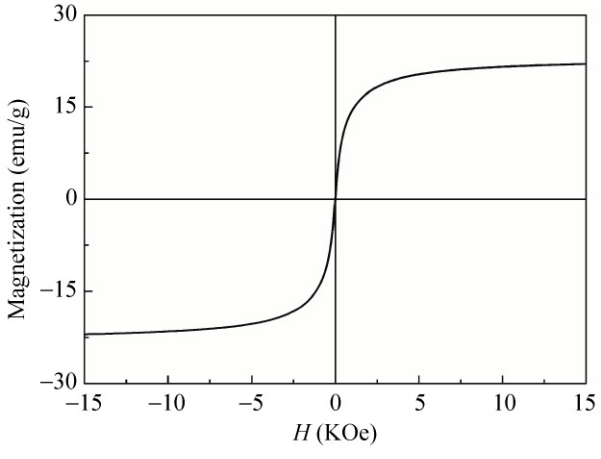

Figure 4 The room-temperature hysteresis loops of $CoPt_3$ NCs prepared using oleylamine as solvent. The $CoPt_3$ NCs show superparamagnetic characteristics at room temperature

structure using $CoPt_3$ NCs as catalysts. Typical morphologies and microstructures of the BNWs are shown in Fig. 5. Large-scale BNWs were found on a Si (111) substrate after growth for 2 h. The diameter of the BNWs had a narrow distribution. The nanowires were tens of micrometers long and 30–50 nm wide, with random growth directions (Figs. 5(a) and 5(b)). In Fig. 5(c), the presence of a catalyst particle at the tip of a nanowire is good proof of a vapor–liquid–solid (VLS) mechanism, in which the liquid–solid interface offers a preferential end of nanowire growth. Above a temperature of 850 ℃, $CoPt_3$ separates into a solid solution of Co and Pt, both of which serve as catalysts. The latter even affords a continuous liquid phase until 1100 ℃ according to Co–Pt, Co–B, and Pt–B binary phase diagrams [29]. In the case of Fe_3O_4, the actual catalytic element is Fe itself, which has a higher eutectic temperature and much smaller corresponding liquid phase area [29]. The detailed crystal structure of the nanowires was further characterized by TEM,

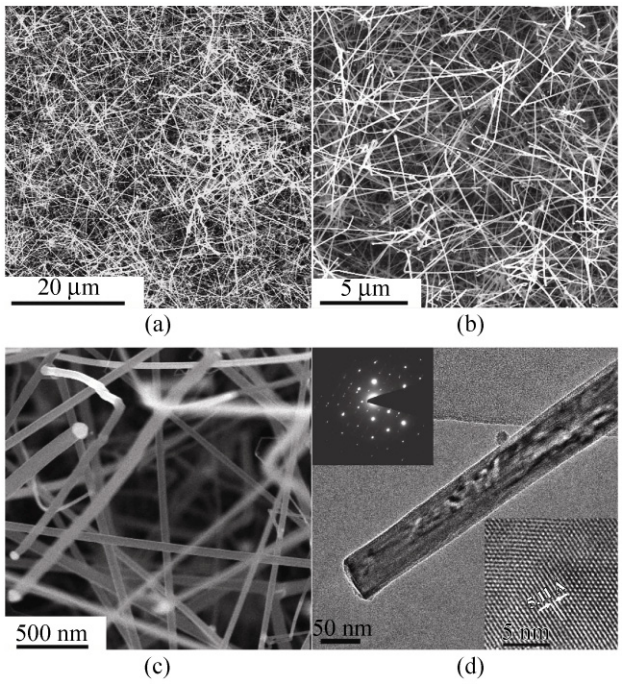

Figure 5 Typical SEM and TEM images of boron nanowires grown using $CoPt_3$ NCs as a catalyst; (a) low magnification SEM image of boron nanowires; (b) high magnification SEM image; (c) high resolution SEM image of boron nanowires; (d) TEM image of a single boron nanowire; the lower right-hand corner inset shows a HRTEM image of the boron nanowire; the top left-hand corner inset shows the SAED pattern of the boron nanowire

HRTEM, and selected area electron diffraction (SAED). The results are shown in Fig. 5(d). The diameters of the BNWs are about 50 nm. The diameters of the BNWs are consistent with the size of $CoPt_3$ catalyst NPs after aggregation at high temperature, which resulted in an increase in the size of the NPs (see Fig. S-1 in the Electronic Supplementary Material (ESM)). The HRTEM image of a BNW indicates that the nanowire has clear lattice fringes and the spacing d between the adjacent growth planes is 0.511 nm, which matches well with the value of the {121} facet of the rhomb-centered hexagonal boron structure from the JCPDS card (PDF #85-0409) [30]. The SAED pattern of BNW (the inset of Fig. 5(d)) shows that it has a single crystalline structure as indicated by the sharp diffraction spots. HRTEM and SAED analysis indicate the growth direction of the BNWs is along {121}.

A modified FE-SEM system was used to perform field emission analyses on the $CoPt_3$ NC-catalyzed BNW films. The sample, as a cathode, was first attached to the side face of a stainless steel triangular prism with conductive glue, then passed and fixed into a 5D direction controller by a magnetic sample transfer pole. A molybdenum probe with tip diameter of 1 mm located in the vacuum chamber functioned as an anode. During the measurements the vacuum gap between the two electrodes was set to 200 μm by a stepper with 10 μm accuracy while the base pressure was maintained at 2.1×10^{-5} Pa. The emission current was measured by a picoammeter (Keithley 485) with a ballast resistor of 10 MΩ, which was used to protect the apparatus against high current discharge. Figure 6(a) shows the relationship between current density J and applied field E. It can be seen that the turn-on field (defined as the applied field at 10 μA/cm² current density) is 9.0 V/μm and the threshold field (defined as the applied field at 1 mA/cm² current density) is 14 V/μm. This turn-on field value of BNWs is higher than that of graphitic nanocones（4 V/μm) [31], and ZnO nanoroses (4.3 V/μm)[32], but better than that of other reported nanostructures including In_2O_3 nanowires (10.7 V/μm) [33], AlN nanocones (12 V/μm) [34], and GaN nanowires (5.9 V/μm) [35]. The screening effect of the high density of BNWs, the random growth directions of the emitters, and oxidation of the silicon substrate surface during the experiment due to the unavoidable presence of traces of oxygen, are possible explanations for the moderate turn-on field. Tip morphology, vacuum degree and vacuum gap may also account for the field emission characteristics.

The J–E relationship was analyzed by the well-known Fowler–Nordheim (F–N) theory for semiconductors, described by the equation [33, 36–38]:

$$J = A\left(\frac{\beta^2 E^2}{\phi}\right)\exp\left(-\frac{B\phi^{2/3}}{\beta E}\right)\exp\left(-\frac{\Delta W^S - \Delta W^P}{2kT}\right)$$

where J is the emission current density, E is the applied electric field, ϕ is the work function of emitter (ϕ_B = 4.5 eV), and A and B are constants with values of $1.5 \times 10^{-6} \times \exp\left(\frac{10.4}{\sqrt{\phi}}\right)$ and 6.44×10^7, respectively. β is usually called the field emission enhancement factor and reflects the ability of an emitter to enhance the local electric field at the tip. The last exponential is a correction of the surface potential configuration, which

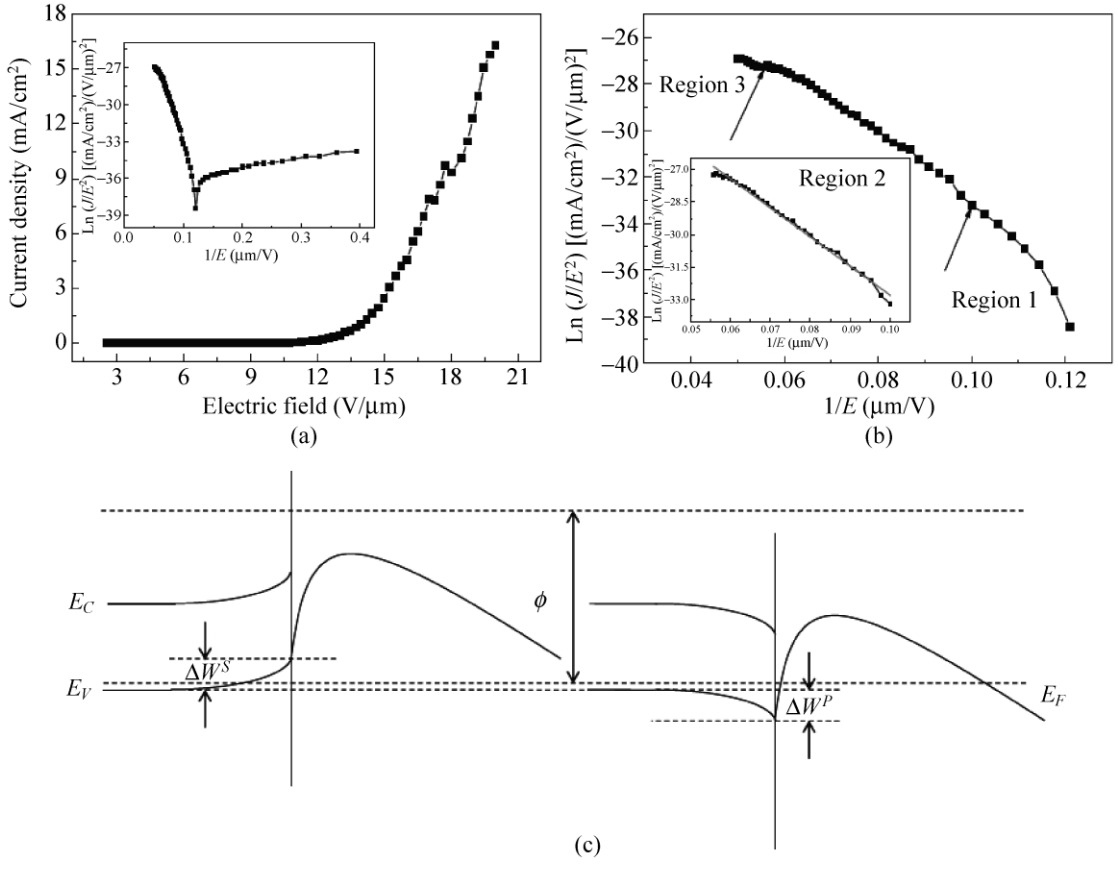

Figure 6 (a) Field emission *J-E* curve of the boron nanowires; the inset is the corresponding F–N plot. (b) Three regions of the F–N plot; the inset is the linear fit of region 2. (c) Energy band diagram near the surface of p type semiconductor affected by surface states and field penetration, the competition between which two leads to the existence of 3 regions in F-N plot (b)

is very important as far as the tunneling of electrons is concerned. k is the Boltzmann constant and T is the absolute temperature. ΔW^S is the surface potential barrier increment due to surface states from absorption of impurity atoms and ΔW^P is the surface potential barrier decrement resulting from field penetration without surface screening. The plot of ln (J/E^2) against $1/E$ for the BNW film (in the insert of Fig. 6(a)) is characteristic of a standard field emission process. Before the inflexion, the curve is a good fit with the F–N model which means that the current originates from electron tunneling through the surface barriers reduced by the external electric field. This F–N plot can be roughly divided in to three regions, as indicated by arrows in Fig. 6(b). Region 1 corresponds to a low electric field, where field emission is dominated by the screening of surface states. In region 3, the field penetration finally breaks down the surface potential barrier and governs the field emission. Region 2 is a transition state between regions 1 and 3, where the current rises rapidly with applied field. This is a result of competition between screening of surface states and field penetration. The enhancement factor β estimated according to the slope k of linear region 2, where $k = \frac{-6.44\times10^7 \phi^{2/3}}{\beta}$, is about 10^3.

4. Conclusions

Monodisperse $CoPt_3$ NCs have been synthesized in an oleylamine solution by an organic solvothermal method. The $CoPt_3$ NCs are ellipsoidal particles with diameters of ca. 6.6 nm and lengths of ca. 10 nm. The $CoPt_3$ NCs have a good single crystal structure. Using $CoPt_3$ NCs as a catalyst, high density and single crystalline BNWs have been successfully fabricated

through a carbon thermal reduction CVD route using C/B/B_2O_3 mixed powders as precursors in an H_2/Ar mixed gas environment at a reaction temperature of 1100 ℃. The BNWs have a diameter of 30–50 nm and a *β*-rhombohedral structure with a growth direction of {121}. BNW thin films have good field emission characteristics. These experimental results suggest that the BNWs are promising can- didates for use in nanoscale cool cathode materials in flat panel display devices.

Acknowledgements

The project was supported by the Natural Science Foundation of China (Grant Nos. 50872147, U0734003), and the National "863" (No. 2007AA03Z305) and "973" (No. 2007CB935503) Projects of the Ministry of Science and Technology of China.

Electronic Supplementary Material: Supplementary material (details of the synthesis of the boron nanowires and their SEM image and EDX pattern) is available in the online version of this article at http://dx.doi.org/10.1007/s12274-011-0134-9 and is accessible free of charge.

References

[1] Leslie-Pelecky, D. L.; Rieke, R. D. Magnetic properties of nanostructured materials. *Chem. Mater.* **1996**, *8*, 1770–1783.

[2] Frey, N. A.; Peng, S.; Cheng, K.; Sun, S. H. Magnetic nanoparticles: Synthesis, functionalization, and applications in bioimaging and magnetic energy storage. *Chem. Soc. Rev.* **2009**, *38*, 2532–2542.

[3] Jun, C. H.; Park, Y. J.; Yeon, Y. R.; Choi, J. R.; Lee, W. R.; Ko, S. J.; Cheon, J. Demonstration of a magnetic and catalytic Co@Pt nanoparticle as a dual-function nanoplatform. *Chem. Commun.* **2006**, 1619–1621.

[4] Mazumder, V.; Chi, M. F.; More, K. L.; Sun, S. H. Core/shell Pd/FePt nanoparticles as an active and durable catalyst for the oxygen reduction reaction. *J. Am. Chem. Soc.* **2010**, *132*, 7848–7849.

[5] Chen, Q. S.; Sun, S. G.; Zhou, Z. Y.; Chen, Y. X.; Deng, S. B. CoPt nanoparticles and their catalytic properties in electrooxidation of CO and CH_3OH studied by *in situ* FTIRS. *Phys. Chem. Chem. Phys.* **2008**, *10*, 3645–3654.

[6] Martins, M. A.; Neves, M. C.; Esteves, A. C. C.; Girginova, P. I.; Guiomar, A. J.; Amaral, V. S.; Trindade, T. Biofunctionalized ferromagnetic $CoPt_3$/polymer nanocomposites. *Nanotechnology* **2007**, *18*, 215609.

[7] Pankhurst, Q. A.; Connolly, J.; Jones, S. K.; Dobson, J. Applications of magnetic nanoparticles in biomedicine. *J. Phys. D: Appl. Phys.* **2003**, *36*, R167–R181.

[8] Shapiro, E. M.; Skrtic, S.; Sharer, K.; Hill, J. M.; Dunbar, C. E.; Koretsky, A. P. MRI detection of single particles for cellular imaging. *Proc. Natl. Acad. Sci.* **2004**, *101*, 10901–10906.

[9] Lee, J. H.; Huh, Y. M.; Jun, Y.; Seo, J.; Jang, J.; Song, H. T.; Kim, S.; Cho, E. J.; Yoon, H. G.; Suh, J. S.; Cheon, J. Artificially engineered magnetic nanoparticles for ultra-sensitive molecular imaging. *Nat. Med.* **2007**, *13*, 95–99.

[10] Wiekhorst, F.; Shevchenko, E.; Weller, H.; Kotzler, J. Anisotropic superparamagnetism of monodispersive cobalt-platinum nanocrystals. *Phys. Rev. B* **2003**, *67*, 224416.

[11] Tzitzios, V.; Niarchos, D.; Margariti, G.; Fidler, J.; Petridis, D. Synthesis of CoPt nanoparticles by a modified polyol method: Characterization and magnetic properties. *Nanotechnology* **2005**, *16*, 287–291.

[12] Alloyeau, D.; Ricolleau, C.; Mottet, C.; Oikawa, T.; Langlois, C.; Le Bouar, Y.; Braidy, N.; Loiseau, A. Size and shape effects on the order-disorder phase transition in CoPt nanoparticles. *Nat. Mater.* **2009**, *8*, 940–946.

[13] Mandal, M.; Das, B.; Mandal, K. Synthesis of CoxPt1-x alloy nanoparticles of different phase by micellar technique and their properties study. *J. Colloid Interface Sci.* **2009**, *335*, 40–43.

[14] Salgado, J. R. C.; Antolini, E.; Gonzalez, E. R. Carbon supported Pt70Co30 electrocatalyst prepared by the formic acid method for the oxygen reduction reaction in polymer electrolyte fuel cells. *J. Power Sources* **2005**, *141*, 13–18.

[15] Wang, C.; van der Vilet, D.; Chang, K. C.; You, H. D.; Strmcnik, D.; Schlueter, J. A.; Markovic, N. M.; Stamenkovic, V. R. Monodisperse Pt_3Co nanoparticles as a catalyst for the oxygen reduction reaction: Size-dependent activity. *J. Phys. Chem. C* **2009**, *113*, 19365–19368.

[16] Stamenkovic, V. R.; Mun, B. S.; Arenz, M.; Mayrhofer, K. J. J.; Lucas, C. A.; Wang, G. F.; Ross, P. N.; Markovic, N. M. Trends in electrocatalysis on extended and nanoscale Pt-bimetallic alloy surfaces. *Nat. Mater.* **2007**, *6*, 241–247.

[17] Jun, Y. W.; Choi, J. S.; Cheon, J. Heterostructured magnetic nanoparticles: Their versatility and high performance capabilities. *Chem. Commun.* **2007**, 1203–1214.

[18] Kockrick, E.; Schmidt, F.; Gedrich, K.; Rose, M.; George, T. A.; Freudenberg, T.; Kraehnert, R.; Skomski, R.; Sellmyer,

D. J.; Kaskel, S. Mesoporous ferromagnetic MPt@silica/carbon (M = Fe, Co, Ni) composites as advanced bifunctional catalysts. *Chem. Mater.* **2010**, *22*, 1624–1632.

[19] Schaffel, F.; Schunemann, C.; Rummeli, M. H.; Taschner, C.; Pohl, D.; Kramberger, C.; Gemming, T.; Leonhardt, A.; Pichler, T.; Rellinghaus, B.; Buchner, B.; Schultz, L. Comparative study on thermal and plasma enhanced CVD grown carbon nanotubes from gas phase prepared elemental and binary catalyst particles. *Phys. Stat. Sol. B* **2008**, *245*, 1919–1922.

[20] Sorge, K. D.; Klein, K. L.; Melechko, A. V.; Finkel, C. L.; Malkina, O.; Leventouri, T.; Fowlkes, J. D.; Rack, P. D.; Simpson, M. L. Magnetic properties of Fe–Co catalysts used for carbon nanofiber synthesis. *J. Appl. Phys.* **2008**, *104*, 033909.

[21] Han, C. Y.; Xiao, Z. L.; Wang, H. H.; Lin, X. M.; Trasobares, S.; Cook, R. E. Facile synthesis of highly aligned multiwalled carbon nanotubes from polymer precursors. *J. Nanomaterials* **2009**, 1–11.

[22] Coquay, P.; Peigney, A.; De Grave, E.; Flahaut, E.; Vandenberghe, R. E.; Laurent, C. Fe/Co alloys for the catalytic chemical vapor deposition synthesis of single- and double-walled carbon nanotubes (CNTs). 1. The CNT-Fe/Co-MgO system. *J. Phys. Chem. B* **2005**, *109*, 17813–17824.

[23] Moshfegh, A. Z. Nanoparticle catalysts. *J. Phys. D: Appl. Phys.* **2009**, *42*, 233001.

[24] Shevchenko, E. V.; Talapin, D. V.; Rogach, A. L.; Kornowski, A.; Haase, M.; Weller, H. Colloidal synthesis and self-assembly of $CoPt_3$ nanocrystals. *J. Am. Chem. Soc.* **2002**, *124*, 11480–11485.

[25] Park, J. I.; Cheon, J. Synthesis of "solid solution" and "core-shell" type cobalt-platinum magnetic nanoparticles via transmetalation reactions. *J. Am. Chem. Soc.* **2001**, *123*, 5743–5746.

[26] Chinnasamy, C. N.; Jeyadevan, B.; Shinoda, K.; Tohji, K. Polyol-process-derived CoPt nanoparticles: Structural and magnetic properties. *J. Appl. Phys.* **2003**, *93*, 7583–7585.

[27] Gibot, P.; Tronc, E.; Chaneac, C.; Jolivet, J. P.; Fiorani, D.; Testa, A. M. (Co,Fe)Pt nanoparticles by aqueous route; self-assembling, thermal and magnetic properties. *J. Magn. Magn. Mater.* **2005**, *290*, 555–558.

[28] Shen, C. M.; Hui, C.; Yang, T. Z.; Xiao, C. W.; Chen, S. T.; Ding, H.; Gao, H. J. Monodispersive CoPt nanoparticles synthesized using chemical reduction method. *Chin. Phys. Lett.* **2008**, *25*, 1479–1481.

[29] Massalski, T. B.; Okamoto, H.; Subramanian, P. R.; Kacprzak, L. *Binary Alloy Phase Diagrams 2nd edn;* ASM International, Materials Park: Ohio, 1990, 3.

[30] JCPDS-International Center for Diffraction Data, PCPDFWIN, v.2.1, 2000.

[31] Lu, X.; Yang, Q.; Xiao, C.; Hirose, A. Field electron emission of carbon-based nanocone films. *Appl. Phys. A* **2006**, *82*, 293–296.

[32] Xu, L. L.; Wu, X. L.; Xiong, X.; Zhu, J.; Chen, H. T.; Huang, G. S.; Chu, P. K. Synthesis and field-emission properties of roselike ZnO nanostructures. *Appl. Phys. A* **2008**, *91*, 247–250.

[33] Li, S. Q.; Liang, Y. X.; Wang, T. H. Nonlinear characteristics of the Fowler–Nordheim plot for field emission from In_2O_3 nanowires grown on InAs substrate. *Appl. Phys. Lett.* **2006**, *88*, 053107.

[34] Liu, C.; Hu, Z.; Wu, Q.; Wang, X.; Chen, Y.; Sang, H.; Zhu, J.; Deng, S.; Xu, N. Vapor−solid growth and characterization of aluminum nitride nanocones. *J. Am. Chem. Soc.* **2005**, *127*, 1318–1322.

[35] Chen, C. C.; Yeh, C. C.; Chen, C. H.; Yu, M. Y.; Liu, H. L.; Wu, J. J.; Chen, K. H.; Chen, L. C.; Peng, J. Y.; Chen, Y. F. Catalytic growth and characterization of gallium nitride nanowires. *J. Am. Chem. Soc.* **2001**, *123*, 2791–2798.

[36] Fowler, R. H.; Nordheim, L. Electron emission in intense electric fields. *Proc. R. Soc. London Ser. A* **1928**, *119*, 173–181.

[37] Stratton, R. Field emission from semiconductors. *Proc. Phys. Soc. B* **1955**, *68*, 746–757.

[38] Wang, X. J.; Tian, J. F.; Yang, T. Z.; Bao, L. H.; Hui, C.; Liu, F.; Shen, C. M.; Gu, C. Z.; Xu, N. S.; Gao, H. J. Single crystalline boron nanocones: Electric transport and field emission properties. *Adv. Mater.* **2007**, *19*, 4480.